Nonlinear inversion for effective stress sensitive parameter using observed seismic data

Huaizhen Chen*, Junxiao Li, and Kristopher A. Innanen

ABSTRACT

Estimation of effective stress has become an important task in reservoir characterization and can guide the selection of fracturing area in unconventional hydrocarbon reservoirs. Based on Gassmann's fluid substitution model, we propose a workflow of employing observed seismic data to implement nonlinear inversion for dry rock moduli, fluid factor and stress-sensitive parameter. We first make an approximation of fluid substitution equation, in which we replace the porosity term with a stress-sensitive parameter. Using stiffness parameters related to the stress-sensitive parameter, we derive a linearized reflection coefficient as a function of reflectivity of stress-sensitive parameter, and we also transfer the reflection coefficient to elastic impedance (EI). The proposed workflow involves estimating EI datasets from seismic data stacked over different ranges of incidence angle and utilizing the estimated EI to implement the inversion for the stress-sensitive parameter. We stress that a model-based least-squares inversion algorithm is used to implement the estimation of EI, and a nonlinear inversion approach is employed to estimate the unknown variables from the estimated EI, which is implemented as a four-step inversion. Synthetic data generated using Zoeppritz equation are utilized to verify the stability of the proposed approach. A test on real data set acquired over a gas-bearing reservoir reveals that the propose workflow appears to preserve as a useful tool to provide reliable results for fluid identification and stress prediction.

INTRODUCTION

Fracturing has been an important tool in the development of unconventional reservoirs (e.g. shale and tight sand reservoirs). Reliable estimation of subsurface effective stress becomes a significant task, which may guide selection of fracturing area and design of drilling trajectory. Effective stress is related to vertical stress and pore pressure. One procedure to predict effective stress is first estimating vertical stress and pore pressure separately and then calculating the effective stress using the estimated results of vertical stress and pore pressure; hence, the accuracy of the effective stress prediction is affected by both the vertical stress estimation and the pore pressure calculation. The other procedure is relating reservoir properties (e.g. porosity) to stress parameter. In the present study, based on a relation between porosity and effective stress (Athy, 1930; Zoback, 2010), we will relate elastic properties (bulk and shear moduli, P- and S-wave velocities, etc.) to stress-sensitive parameter.

Gassmann (1951) proposed a fluid substitution equation to compute effective bulk and shear moduli for saturated rocks, in which the effective bulk modulus is related to mineral bulk modulus, porosity, dry rock bulk modulus and fluid bulk modulus. Krief et al. (1990) proposed a nonlinear equation to calculate the bulk modulus of dry rock using the total porosity. Based on the critical porosity (CP) model proposed by Nur et al. (1998), a linear relationship is proposed to compute the bulk modulus of dry rock using the total porosity

and the critical porosity (Mavko et al., 2009). Combining the linear relationship between dry rock bulk modulus and porosity and the relation between porosity and effective stress, we will re-express the fluid substitution equation in terms of the dry rock bulk modulus and the effective stress-sensitive parameter.

In order to estimate stress-sensitive parameter from observed seismic data, a reflection coefficient related to stress is required. Shaw and Sen (2006) proposed a relationship between perturbation in stiffness matrix and linearized reflection coefficients. After obtaining the re-expressed fluid substitution equation, we may derive the stiffness matrix using the stress related bulk modulus of saturated rocks. With the derived stiffness matrix in hand, we express the perturbation in each stiffness parameter in the case of an interface separating two layers and obtain a linearized P-to-P reflection coefficient as a function of stress-sensitive parameter. Based on the reflection coefficient, elastic impedance (EI) is also formulated, which will become the foundation for establishing nonlinear inversion algorithm.

Full waveform inversion (FWI) has been widely studied for estimating elastic parameters. Possibility of combining amplitude versus offset (AVO) and FWI is investigated by Innanen (2014), in which the approximation of inverse Hessian matrix for different parameterizations is proposed. The procedure to implement the FWI is iteratively minimizing errors between observed datasets and synthetic results generated using the estimated model and forward modeling (Pan et al., 2017), and in FWI the calculation of gradient and Hessian matrices is complicated (Innanen, 2014; Pan et al., 2018). In the present study, we aim to establish a nonlinear inversion approach to estimate elastic properties and stress-sensitive parameter using observed seismic data based on the procedure of FWI. Novel parts of the inversion approach involves: 1) results of EI are employed as the input in the nonlinear inversion, and 2) gradients of EI with respect to unknown variables are clearly expressed. We finally apply the proposed inversion approach to synthetic and real data to verify the stability and reliability of estimating elastic properties and stress-sensitive parameters.

THEORY AND METHOD

Elastic properties related to effective stress

Based on Gassmann (1951) fluid substitution model, the low-frequency saturated rock bulk modulus, K_{sat}, is given by (Mavko et al., 2009)

$$K_{\mathrm{sat}} = K_{\mathrm{dry}} + \frac{\left(1 - K_{\mathrm{dry}}/K_0\right)^2}{\phi/K_{\mathrm{f}} + (1-\phi)/K_0 - K_{\mathrm{dry}}/K_0^2}, \tag{1}$$

where ϕ is the porosity, K_{f} is the effective bulk modulus of filling fluid, and K_{dry} and K_0 are effective bulk moduli of dry rock and minerals that makes up the rock, respectively. Nur et al. (1998) proposed a critical porosity (CP) model, from which relationship between the effect bulk modulus of dry rock K_{dry} and porosity ϕ is given by

$$K_{\mathrm{dry}} = K_0 \left(1 - \frac{\phi}{\phi_{\mathrm{c}}}\right), \tag{2}$$

where ϕ_{c} is the critical porosity, which separates the consolidated rock domain from the suspension domain.

We next model variation of dry rock bulk modulus ($K_{\rm dry}$) with porosity, and compare the result of $K_{\rm dry}$ calculated using the critical model and that computed using Krief's equation (Krief et al., 1990) in the case of different values of clay volume and critical porosity, as plotted in Figure 1. It is important to stress that we employ Voigt-Reuss-Hill average model (Mavko et al., 2009) to compute the effective bulk and shear moduli of minerals (i.e. K_0 and μ_0) in the present study.

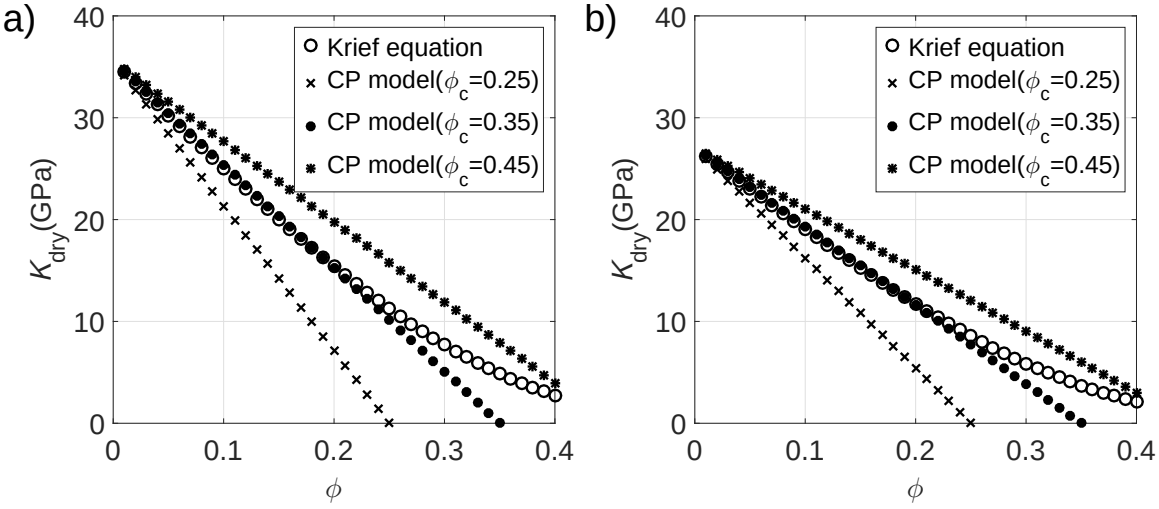

FIG. 1. Variations of dry rock bulk modulus with with porosity, and comparisons between results computed using CP model and that calculated using Krief's equation in the case of different values of critical porosity. Minerals making up the rock are clay and quartz. a) Clay volume $V_{\rm clay}$ is 0.1, and b) Clay volume $V_{\rm clay}$ is 0.8.

From the comparison, we observe that there is a good match between results of dry rock bulk modulus computed using the critical model and those calculated using Krief's equation in the case of $\phi_{\rm c}$ is 0.35 and the porosity is less than 0.2; hence, we let the critical porosity $\phi_{\rm c}$ approximately be 0.35 in the present study. Substituting equation 2 into equation 1 yields

$$\begin{aligned} K_{\rm sat} &= K_{\rm dry} + \frac{\left(\phi/\phi_{\rm c}\right)^2}{\phi/K_{\rm f} + \left(1-\phi\right)/K_0 - \left(1-\frac{\phi}{\phi_{\rm c}}\right)/K_0} \\ &= K_{\rm dry} + \frac{K_0\left(\phi/\phi_{\rm c}\right)^2}{\phi K_0/K_{\rm f} - \left(\phi - \frac{\phi}{\phi_{\rm c}}\right)}. \end{aligned} \tag{3}$$

Because $K_0 \gg K_{\rm f}$, we assume $\phi K_0/K_{\rm f} \gg \left(\phi - \frac{\phi}{\phi_{\rm c}}\right)$, and we may simply equation 3 as

$$K_{\rm sat} \approx K_{\rm dry} + \frac{\phi}{\left(\phi_{\rm c}\right)^2} K_{\rm f}. \tag{4}$$

We next relate the effective bulk modulus of saturated rock $K_{\rm sat}$ to effective stress $\sigma_{\rm e}$ by involving the stress dependent porosity $\phi(\sigma_{\rm e})$. Smith (1971) proposed a simple exponential porosity-effective stress function as

$$\phi \approx \phi_0 P_{\rm e}, \tag{5}$$

where P_{e} is a stress-sensitive parameter, $P_{\mathrm{e}} = \exp(-a\sigma_{\mathrm{e}})$, a is related to rock compaction, and ϕ_0 is the initial porosity, which is assumed to be equal to ϕ_{c} in the present study. Following Hantschel and Kauerauf (2009), we assume parameter a to be 0.03. Substituting equation 5 into equation 4 yields

$$K_{\mathrm{sat}} \approx K_{\mathrm{dry}} + \frac{K_{\mathrm{f}}}{\phi_{\mathrm{c}}} P_{\mathrm{e}}. \tag{6}$$

Combining equations 3 and 6, we first plot variations of stress-sensitive parameter with porosity and water saturations in the case of different values of clay volumes in Figure 2. Effective bulk modulus of fluid (the mixture of water and gas) is computed using Wood's equation (Mavko et al., 2009). We observe the stress-sensitive parameter increases with porosity, and decreases as water saturation increases. From comparisons between P_{e} results computed for the case of different values of clay volume, we conclude the variation of stress-sensitive parameter with porosity and water saturation in shale rocks is much similar to that in sand rocks.

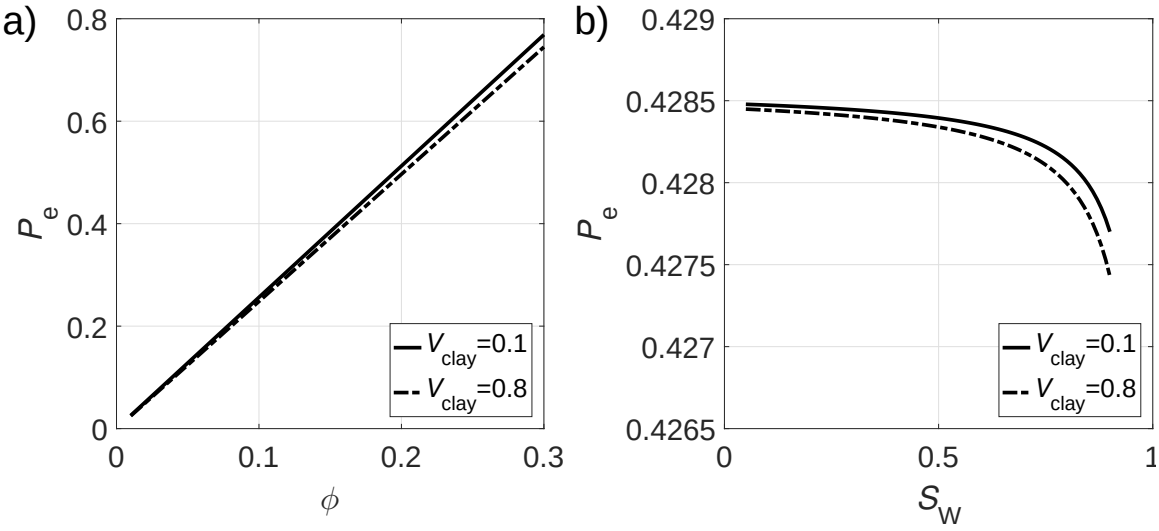

FIG. 2. Variation of stress-sensitive parameter P_{e} with porosity ϕ and water saturation S_{W}. a) Variation of P_{e} with porosity; b) Variation of P_{e} with water saturation.

Given different values of porosity and water saturation, we may compute the effective bulk modulus of saturated rock, and we also compare the result computed using equation 6 and that calculated using Gassmann's equation (equation 1), as shown in Figure 3. We observe that the difference between the result calculated using Gassmann's equation and that computed using approximate formula increases with the porosity, and the effect of water saturation on the difference is relatively small in the case of $\phi \leq 0.2$. It indicates that the approximate formula is acceptable in the case that ϕ is less than 0.2. Based on Gassmann's model, we also assume the effective shear modulus of saturated rock to be equal to that of dry rock (i.e. $\mu = \mu_{\mathrm{sat}} = \mu_{\mathrm{dry}}$). The shear modulus μ is calculated by

$$\mu = \mu_0 \left(1 - \frac{\phi}{\phi_{\mathrm{c}}}\right), \tag{7}$$

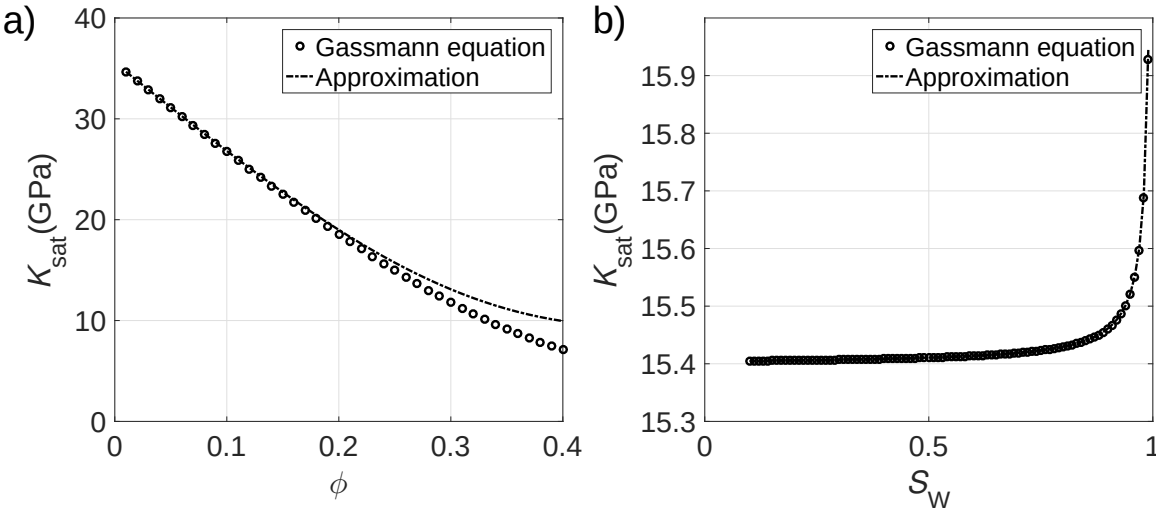

FIG. 3. Comparisons between results of saturated rock bulk modulus computed using Gassmann's equation and those calculated using approximate formula (equation 6). a) Water saturation S_{W} is 1, and clay volume is 0.1; b) Clay volume is 0.1, and rock porosity ϕ is 0.2.

where μ_0 is the effective shear modulus of minerals making up the rock. We next involve the effect of stress in the rock stiffness matrix

$$\mathbf{C} = \begin{bmatrix} C_{33} & C_{33}-2C_{55} & C_{33}-2C_{55} & 0 & 0 & 0 \\ C_{33}-2C_{55} & C_{33} & C_{33}-2C_{55} & 0 & 0 & 0 \\ C_{33}-2C_{55} & C_{33}-2C_{55} & C_{33} & 0 & 0 & 0 \\ 0 & 0 & 0 & C_{55} & 0 & 0 \\ 0 & 0 & 0 & 0 & C_{55} & 0 \\ 0 & 0 & 0 & 0 & 0 & C_{55} \end{bmatrix}, \tag{8}$$

where $C_{33} = K_{\mathrm{sat}} + \frac{4}{3}\mu$, and $C_{55} = \mu$.

P-to-P linearized reflection coefficient

A relationship between the scattering function S and the P-to-P reflection coefficient R_{PP} is given by (Shaw and Sen, 2006)

$$R_{\mathrm{PP}} = \frac{1}{4\rho\cos^2\theta} S, \tag{9}$$

where ρ is density of a reference medium, and θ is P-wave incidence angle. The scattering function S is related to perturbation in density and stiffness parameters

$$\begin{aligned} S =& \Delta\rho\cos 2\theta + \Delta C_{33}\left(\xi_{11}+\xi_{22}+\xi_{33}+\xi_{12}+\xi_{21}+\xi_{13}+\xi_{31}+\xi_{23}+\xi_{32}\right) \\ &+ \Delta C_{55}(\xi_{44}+\xi_{55}+\xi_{66}-2\xi_{12}-2\xi_{21}-2\xi_{13}-2\xi_{31}-2\xi_{23}-2\xi_{32}), \end{aligned} \tag{10}$$

where ξ_{ij} is related to the incidence angle θ given by (Shaw and Sen, 2006), ΔC_{33} and ΔC_{55} are perturbations in stiffness parameters C_{33} and C_{55}, and $\Delta\rho$ is perturbation in density across the reflection interface. Using the derived stiffness matrix shown in equation 8, we next express the perturbation ΔC_{33} as a function of stress. Figure 4 plots a model of reflection interface separating two layers that have different values of effective bulk modulus of dry rock, shear modulus of saturated rock, density and effective stress, in which ΔK_{dry}, $\Delta\mu_{\mathrm{dry}}$ and $\Delta\sigma_{\mathrm{e}}$ represent perturbations in elastic properties and stress across the reflection interface, respectively. The perturbation, ΔC_{33}, is expressed as

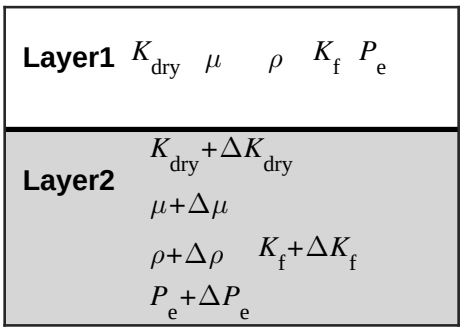

FIG. 4. A model of reflection interface separating two layers.

$$\begin{aligned}\Delta C_{33} =& \left(K_{\rm sat}+\frac{4}{3}\mu\right)_{layer2} - \left(K_{\rm sat}+\frac{4}{3}\mu\right)_{layer1}\\ \approx& K_{\rm dry}+\Delta K_{\rm dry}+\frac{K_{\rm f}+\Delta K_{\rm f}}{\phi_{\rm c}}\left(P_{\rm e}+\Delta P_{\rm e}\right)-\left(K_{\rm dry}+\frac{K_{\rm f}}{\phi_{\rm c}}P_{\rm e}\right)\\ \approx& \Delta K_{\rm dry}+\frac{\Delta K_{\rm f}}{\phi_{\rm c}}P_{\rm e}+\frac{K_{\rm f}}{\phi_{\rm c}}\Delta P_{\rm e},\end{aligned} \tag{11}$$

in which we neglect the term proportional to $\Delta K_{\rm f}\Delta P_{\rm e}$ under the assumption of small changes in fluid bulk modulus and stress-sensitive parameter across the interface. Furthermore, the perturbation in ΔC_{55} is given by

$$\Delta C_{55} = \Delta\mu. \tag{12}$$

Combining equations 9-12, we derive the final expression of P-to-P linearized reflection coefficient as (See Appendix A)

$$\begin{aligned}R_{\rm PP} =& \frac{1}{2\cos^2\theta}\left(\frac{\gamma_{\rm sat}}{\gamma_{\rm dry}}-\frac{4}{3}\gamma_{\rm sat}\right)R_{K_{\rm dry}} - 4\gamma_{\rm sat}\sin^2\theta R_\mu + \frac{\cos 2\theta}{2\cos^2\theta}R_F\\ &+\frac{1}{2\cos^2\theta}\left(2\sin^2\theta-\frac{\gamma_{\rm sat}}{\gamma_{\rm dry}}\right)R_{K_{\rm f}}+\frac{1}{2\cos^2\theta}\left(1-\frac{\gamma_{\rm sat}}{\gamma_{\rm dry}}\right)R_{P_{\rm e}},\end{aligned} \tag{13}$$

where

$$R_{K_{\rm dry}} = \frac{\Delta K_{\rm dry}}{2K_{\rm dry}}, R_\mu = \frac{\Delta\mu}{2\mu}, R_F = \frac{\Delta F}{2F}, R_{K_{\rm f}} = \frac{\Delta K_{\rm f}}{2K_{\rm f}}, R_{P_{\rm e}} = \frac{\Delta P_{\rm e}}{2P_{\rm e}}, \tag{14}$$

and where F is a fluid-sensitive factor, $F = \rho K_{\rm f}$, $\gamma_{\rm sat} = \mu/\left(K_{\rm sat}+4/3\mu\right)$, $K_{\rm sat}$ is computed using equation 6, and $\gamma_{\rm dry} = \mu/\left(K_{\rm dry}+4/3\mu\right)$. The derived reflection coefficient make it possible to model how dry rock properties, fluid and stress affect seismic amplitude variation with offset/angle (AVO/AVA), and based on the derived reflection coefficient, we may estimate dry rock moduli, fluid-sensitive factor, and stress-sensitive parameter using observed seismic data.

Nonlinear inversion for dry rock elastic properties, fluid factor, and stress-sensitive parameter based on elastic impedance

Based on the derived reflection coefficient, we proceed to seismic inversion for dry rock bulk modulus, fluid-sensitive factor and stress-sensitive parameter. We first replace

the reflection coefficient, R_{PP}, and reflectivities, $R_{K_{\mathrm{dry}}}$, R_{μ}, R_{F}, $R_{K_{\mathrm{f}}}$, and $R_{P_{\mathrm{e}}}$, with the following assumptions

$$\begin{aligned} &R_{\mathrm{PP}} = \frac{1}{2}\frac{\Delta \mathrm{EI}}{\mathrm{EI}} \approx \frac{1}{2}\Delta \ln\left(\mathrm{EI}\right), R_{K_{\mathrm{dry}}} \approx \frac{1}{2}\Delta \ln\left(K_{\mathrm{dry}}\right), R_{\mu} \approx \frac{1}{2}\Delta \ln\left(\mu\right), \\ &R_{F} \approx \frac{1}{2}\Delta \ln\left(F\right), R_{K_{\mathrm{f}}} \approx \frac{1}{2}\Delta \ln\left(K_{\mathrm{f}}\right), R_{P_{\mathrm{e}}} \approx \frac{1}{2}\Delta \ln\left(P_{\mathrm{e}}\right), \end{aligned} \tag{15}$$

where EI is elastic impedance (Connolly, 1999; Whitcombe, 2002; Chen et al., 2018). Substituting equation 15 into equation 13 yields

$$\begin{aligned} \Delta \ln\left(\mathrm{EI}\right) =& \frac{1}{2\cos^2\theta}\left(\frac{\gamma_{\mathrm{sat}}}{\gamma_{\mathrm{dry}}} - \frac{4}{3}\gamma_{\mathrm{sat}}\right)\Delta \ln\left(K_{\mathrm{dry}}\right) - 4\gamma_{\mathrm{sat}}\sin^2\theta\Delta \ln\left(\mu\right) + \frac{\cos 2\theta}{2\cos^2\theta}\Delta \ln\left(F\right) \\ &+ \frac{1}{2\cos^2\theta}\left(2\sin^2\theta - \frac{\gamma_{\mathrm{sat}}}{\gamma_{\mathrm{dry}}}\right)\Delta \ln\left(K_{\mathrm{f}}\right) + \frac{1}{2\cos^2\theta}\left(1 - \frac{\gamma_{\mathrm{sat}}}{\gamma_{\mathrm{dry}}}\right)\Delta \ln\left(P_{\mathrm{e}}\right). \end{aligned} \tag{16}$$

Taking an integral on both sides of the equation and removing the logarithmic terms, we obtain the expression of EI

$$\mathrm{EI} = \mathrm{EI}_0\left(\frac{K_{\mathrm{dry}}}{K_{\mathrm{dry0}}}\right)^{a_{K_{\mathrm{dry}}}(\theta)}\left(\frac{\mu}{\mu_0}\right)^{a_{\mu}(\theta)}\left(\frac{F}{F_0}\right)^{a_{F}(\theta)}\left(\frac{K_{\mathrm{f}}}{K_{\mathrm{f0}}}\right)^{a_{K_{\mathrm{f}}}(\theta)}\left(\frac{P_{\mathrm{e}}}{P_{\mathrm{e0}}}\right)^{a_{P_{\mathrm{e}}}(\theta)}, \tag{17}$$

where $a_{K_{\mathrm{dry}}}\left(\theta\right) = \frac{1}{2\cos^2\theta}\left(\frac{\gamma_{\mathrm{sat}}}{\gamma_{\mathrm{dry}}} - \frac{4}{3}\gamma_{\mathrm{sat}}\right)$, $a_{\mu}\left(\theta\right) = -4\gamma_{\mathrm{sat}}\sin^2\theta$, $a_{F}\left(\theta\right) = \frac{\cos 2\theta}{2\cos^2\theta}$, $a_{K_{\mathrm{f}}}\left(\theta\right) = \frac{1}{2\cos^2\theta}\left(2\sin^2\theta - \frac{\gamma_{\mathrm{sat}}}{\gamma_{\mathrm{dry}}}\right)$, $a_{P_{\mathrm{e}}}\left(\theta\right) = \frac{1}{2\cos^2\theta}\left(1 - \frac{\gamma_{\mathrm{sat}}}{\gamma_{\mathrm{dry}}}\right)$, $\mathrm{EI}_0 = \alpha_0\rho_0$, α_0 and ρ_0 are constants of P-wave velocity and density, and K_{dry0}, μ_0, F_0, K_{f0} and P_{e0} are also constants of corresponding variables, which are calculated using well log data (Whitcombe, 2002). Relationship between vector of seismic data and EI in case of n reflection interface is given by

$$\mathbf{S}\left(\theta_i\right) = \mathbf{WDLEI}\left(\theta_i\right), \tag{18}$$

where

$$\begin{aligned} \mathbf{S}\left(\theta_i\right) = \begin{bmatrix} s_1 \\ \vdots \\ s_n \end{bmatrix}_{n\times 1}, \mathbf{W} = \begin{bmatrix} w_1 & 0 & \dots & 0 \\ w_2 & w_1 & \ddots & \vdots \\ \vdots & \vdots & \ddots & 0 \\ w_n & w_{n-1} & \dots & w_1 \end{bmatrix}_{n\times n}, \\ \mathbf{D} = \frac{1}{2}\begin{bmatrix} -1 & 1 & & \\ & -1 & 1 & \\ & & \ddots & \ddots \\ & & & -1 \quad 1 \end{bmatrix}_{n\times(n+1)}, \mathbf{LEI}\left(\theta_i\right) = \begin{bmatrix} \log(\mathrm{EI}_1) \\ \vdots \\ \log(\mathrm{EI}_{n+1}) \end{bmatrix}_{(n+1)\times 1}, \end{aligned} \tag{19}$$

in which $w_1, ..., w_n$ are samples in the extracted source wavelet, $s_1, ..., s_n$ are samples in the input seismic data of incidence angle θ_i, and $\log(\mathrm{EI}_1), ..., \log(\mathrm{EI}_{n+1})$ are samples in logarithmic EI, respectively. Based on equation 18, we may estimate EI datasets from the observed seismic data stacked over different ranges of incidence angle using a model-constrained least-square inversion algorithm which is proposed by Chen et al. (2018). After

obtaining the estimated EI, we proceed to nonlinear inversion for the unknown parameter vector in which dry rock bulk modulus, fluid-sensitive factor and stress-sensitive parameter are involved. A nonlinear relationship between EI and the unknown parameter vector in the case of six incidence angles (θ_1, θ_2, θ_3, θ_4, θ_5 and θ_6) and n reflection interface is given by

$$\mathbf{d} = \mathbf{G}(\mathbf{m}), \tag{20}$$

where

$$\begin{aligned}
\mathbf{d} &= \left[\, \mathbf{EI}(\theta_1)\ \mathbf{EI}(\theta_2)\ \mathbf{EI}(\theta_3)\ \mathbf{EI}(\theta_4)\ \mathbf{EI}(\theta_5)\ \mathbf{EI}(\theta_6) \,\right]^T, \\
\mathbf{m} &= \left[\, \mathbf{K}_{\mathrm{dry}}\ \boldsymbol{\mu}\ \mathbf{F}\ \mathbf{K}_{\mathrm{f}}\ \mathbf{P}_{\mathrm{e}} \,\right]^T, \mathbf{EI} = \left[\, \mathrm{EI}_1\ \ldots\ \mathrm{EI}_{n+1} \,\right]^T, \\
\mathbf{K}_{\mathrm{dry}} &= \left[\, (K_{\mathrm{dry}})_1\ \ldots\ (K_{\mathrm{dry}})_{n+1} \,\right]^T, \boldsymbol{\mu} = \left[\, \mu_1\ \ldots\ \mu_{n+1} \,\right]^T, \\
\mathbf{K}_{\mathrm{f}} &= \left[\, (K_{\mathrm{f}})_1\ \ldots\ (K_{\mathrm{f}})_{n+1} \,\right]^T, \mathbf{F} = \left[\, F_1\ \ldots\ F_{n+1} \,\right]^T, \\
\mathbf{P}_{\mathrm{e}} &= \left[\, (P_{\mathrm{e}})_1\ \ldots\ (P_{\mathrm{e}})_{n+1} \,\right]^T,
\end{aligned} \tag{21}$$

and where subscripts of elements in vectors of unknown parameters and EI represent corresponding layers, and $\mathbf{G}$ is a vector related to parameters before reflectivities.

We assume the vector of estimated EI that is the input for the nonlinear inversion to be $\mathbf{d}_{\mathrm{obs}}$; and given a model $\mathbf{m}_{\mathrm{mod}}$, we obtain the vector of synthetic EI data $\mathbf{d}_{\mathrm{mod}}$. If the data misfit or residual $\delta\mathbf{d} = \mathbf{d}_{\mathrm{mod}} - \mathbf{d}_{\mathrm{obs}}$ is small, the given model $\mathbf{m}_{\mathrm{mod}}$ can be approximately equal to the true model $\mathbf{m}$. Therefore we need to search for the model that makes the data misfit be much smaller to implement the estimation of unknown parameters. The L2-norm of the misfit is given by

$$\mathbf{E} = \|\mathbf{d}_{\mathrm{mod}} - \mathbf{d}_{\mathrm{obs}}\|_2 = \frac{1}{2}(\delta\mathbf{d})^T(\delta\mathbf{d}), \tag{22}$$

where $\mathbf{E}$ represents the energy of the data residual. From equation 22, we observe the estimation of unknown parameter vector has been transfered to the problem of obtaining a model that can make the energy of the data residual be smaller. We employ an iteration procedure to obtain the appropriate model

$$\mathbf{m} = \mathbf{m}_{\mathrm{i}} + \delta\mathbf{m}, \tag{23}$$

where $\delta\mathbf{m}$ is the search direction for each iteration, and $\mathbf{m}_{\mathrm{i}}$ is an initial model, respectively. The main task is to determine the search direction for each iteration. The L2-norm of the misfit is expanded near the starting point in a Taylor series

$$\mathbf{E}(\mathbf{m}_{\mathrm{i}} + \delta\mathbf{m}) \approx \mathbf{E}(\mathbf{m}_{\mathrm{i}}) + \left(\frac{\partial\mathbf{E}}{\partial\mathbf{m}}\right)\delta\mathbf{m} + \frac{1}{2}\left(\frac{\partial^2\mathbf{E}}{\partial^2\mathbf{m}}\right)(\delta\mathbf{m})^2. \tag{24}$$

By solving equation 24, we may obtain the result of $\delta\mathbf{m}$. The derivative on both sides of the equation with respect to $\delta\mathbf{m}$ is given by

$$\frac{\partial\mathbf{E}(\mathbf{m}_{\mathrm{i}} + \delta\mathbf{m})}{\delta\mathbf{m}} = \left(\frac{\partial\mathbf{E}}{\partial\mathbf{m}}\right) + \left(\frac{\partial^2\mathbf{E}}{\partial^2\mathbf{m}}\right)(\delta\mathbf{m}). \tag{25}$$

Letting the derivation be zero, we may obtain the result of $\delta\mathbf{m}$ as

$$\delta\mathbf{m} = -\mathbf{H}^{-1}\mathbf{g}, \tag{26}$$

where $\mathbf{g} = \left(\frac{\partial\mathbf{E}}{\partial\mathbf{m}}\right)$, which represents the gradient of $\mathbf{E}$ with respect to $\mathbf{m}$, $\mathbf{H}$ is the Hessian matrix (Köhn, 2011; Innanen, 2014). Equation 26 implies that prior to computing the direction $\delta\mathbf{m}$ we need to calculate the gradient $\mathbf{g}$. We proceed to the calculation of the gradient of residual energy with respect to $\mathbf{m}$.

$$\frac{\partial\mathbf{E}}{\partial\mathbf{m}} = \frac{\partial\left[\frac{1}{2}\left(\mathbf{d}_{\rm mod}-\mathbf{d}_{\rm obs}\right)^T\left(\mathbf{d}_{\rm mod}-\mathbf{d}_{\rm obs}\right)\right]}{\partial\mathbf{m}} = \frac{\partial\mathbf{d}_{\rm mod}\left(\mathbf{m}\right)}{\partial\mathbf{m}}(\delta\mathbf{d}), \tag{27}$$

in which the gradient of synthetic EI data with respect to $\mathbf{m}$, $\frac{\partial\mathbf{d}_{\rm mod}(\mathbf{m})}{\partial\mathbf{m}}$, is given by

$$\frac{\partial\mathbf{d}_{\rm mod}\left(\mathbf{m}\right)}{\partial\mathbf{m}} = \left[\begin{array}{ccccc}\frac{\partial(\mathbf{EI})}{\partial\left(\mathbf{K}_{\rm dry}\right)} & \frac{\partial(\mathbf{EI})}{\partial(\boldsymbol{\mu})} & \frac{\partial(\mathbf{EI})}{\partial(\mathbf{F})} & \frac{\partial(\mathbf{EI})}{\partial(\mathbf{K}_{\rm f})} & \frac{\partial(\mathbf{EI})}{\partial(\mathbf{P}_{\rm e})}\end{array}\right]^T, \tag{28}$$

where we assume the vectors of variables, $\mathbf{K}_{\rm dry}$, $\boldsymbol{\mu}$, $\mathbf{F}$, $\mathbf{K}_{\rm f}$ and $\mathbf{P}_{\rm e}$, involved in the vector $\mathbf{m}$ are independent of each other. Therefore, substituting equation 17 into equation 28, we obtain the components

$$\begin{aligned}
\frac{\partial\left(\mathbf{EI}\right)}{\partial(\mathbf{K}_{\rm dry})} &= \frac{a_{K_{\rm dry}}\left(\theta\right)\mathrm{EI}_0}{K_{\rm dry0}}\left(\frac{K_{\rm dry}}{K_{\rm dry0}}\right)^{a_{K_{\rm dry}}(\theta)-1}\left(\frac{\mu}{\mu_0}\right)^{a_\mu(\theta)}\left(\frac{F}{F_0}\right)^{a_F(\theta)}\left(\frac{K_{\rm f}}{K_{\rm f0}}\right)^{a_{K_{\rm f}}(\theta)}\left(\frac{P_{\rm e}}{P_{\rm e0}}\right)^{a_{P_{\rm e}}(\theta)},\\
\frac{\partial\left(\mathbf{EI}\right)}{\partial(\boldsymbol{\mu})} &= \frac{a_\mu\left(\theta\right)\mathrm{EI}_0}{\mu_0}\left(\frac{K_{\rm dry}}{K_{\rm dry0}}\right)^{a_{K_{\rm dry}}(\theta)}\left(\frac{\mu}{\mu_0}\right)^{a_\mu(\theta)-1}\left(\frac{F}{F_0}\right)^{a_F(\theta)}\left(\frac{K_{\rm f}}{K_{\rm f0}}\right)^{a_{K_{\rm f}}(\theta)}\left(\frac{P_{\rm e}}{P_{\rm e0}}\right)^{a_{P_{\rm e}}(\theta)},\\
\frac{\partial\left(\mathbf{EI}\right)}{\partial(\mathbf{F})} &= \frac{a_F\left(\theta\right)\mathrm{EI}_0}{F_0}\left(\frac{K_{\rm dry}}{K_{\rm dry0}}\right)^{a_{K_{\rm dry}}(\theta)}\left(\frac{\mu}{\mu_0}\right)^{a_\mu(\theta)}\left(\frac{F}{F_0}\right)^{a_F(\theta)-1}\left(\frac{K_{\rm f}}{K_{\rm f0}}\right)^{a_{K_{\rm f}}(\theta)}\left(\frac{P_{\rm e}}{P_{\rm e0}}\right)^{a_{P_{\rm e}}(\theta)},\\
\frac{\partial\left(\mathbf{EI}\right)}{\partial(\mathbf{K}_{\rm f})} &= \frac{a_{K_{\rm f}}\left(\theta\right)\mathrm{EI}_0}{K_{\rm f0}}\left(\frac{K_{\rm dry}}{K_{\rm dry0}}\right)^{a_{K_{\rm dry}}(\theta)}\left(\frac{\mu}{\mu_0}\right)^{a_\mu(\theta)}\left(\frac{F}{F_0}\right)^{a_F(\theta)}\left(\frac{K_{\rm f}}{K_{\rm f0}}\right)^{a_{K_{\rm f}}(\theta)-1}\left(\frac{P_{\rm e}}{P_{\rm e0}}\right)^{a_{P_{\rm e}}(\theta)},\\
\frac{\partial\left(\mathbf{EI}\right)}{\partial(\mathbf{P}_{\rm e})} &= \frac{a_{P_{\rm e}}\left(\theta\right)\mathrm{EI}_0}{P_{\rm e0}}\left(\frac{K_{\rm dry}}{K_{\rm dry0}}\right)^{a_{K_{\rm dry}}(\theta)}\left(\frac{\mu}{\mu_0}\right)^{a_\mu(\theta)}\left(\frac{F}{F_0}\right)^{a_F(\theta)}\left(\frac{K_{\rm f}}{K_{\rm f0}}\right)^{a_{K_{\rm f}}(\theta)}\left(\frac{P_{\rm e}}{P_{\rm e0}}\right)^{a_{P_{\rm e}}(\theta)-1}.
\end{aligned} \tag{29}$$

EXAMPLES

Well log model construction

With curves of P- and S-wave velocities ($\alpha = \sqrt{\frac{K_{\rm sat}+4/3\mu}{\rho}}$, and $\beta = \sqrt{\frac{\mu}{\rho}}$) and density ρ provided by well log in hand, we may roughly estimate clay volume $V_{\rm clay}$, porosity ϕ and effective stress $\sigma_{\rm e}$ using empirical relations. Castagna et al. (1985) proposed a relationship among P-wave velocity, porosity and clay volume for shaley sands

$$\alpha = 5.81 - 9.42\phi - 2.21V_{\rm clay}. \tag{30}$$

Relationship among saturated rock density ρ, porosity and clay volume is given by (Mavko et al., 2009)

$$\rho = \left[V_{\rm clay}\rho_{\rm clay} + (1 - V_{\rm clay})\,\rho_{\rm quartz}\right](1 - \phi) + \phi\rho_{\rm f}, \tag{31}$$

where $\rho_{\rm f}$ is the density of fluid. Using the values of $\rho_{\rm quartz}$ and $\rho_{\rm clay}$ given by Blangy (1992) ($\rho_{\rm quartz} = 2.65{\rm g/cm}^3$; $\rho_{\rm clay} = 2.55{\rm g/cm}^3$), we rewrite the empirical relationship among density, porosity and clay volume for water-saturated rock

$$\rho \approx 2.65 - 1.65\phi - 0.1V_{\rm clay}, \tag{32}$$

in which we neglect the term proportional to $V_{\rm clay}\phi$. Combining equations 30 and 32, we may utilize P-wave velocity and density to compute porosity and clay volume, and then we employ the computed result of porosity to calculate the stress-sensitive parameter $P_{\rm e}$ using equation 5. The effective bulk and shear moduli of minerals are calculated using the result of clay volume, and the effective bulk and shear moduli of the dry rock are computed based on equations 2 and 7. The bulk modulus of fluid is estimated using equation 4. Following this procedure, when we apply the nonlinear inversion approach to real data sets, we may also employ results of P- and S-wave velocities and density obtained by inversion of pre-stack seismic data using a software package, to roughly estimate the values of $K_{\rm dry}$, μ, F, $K_{\rm f}$ and $P_{\rm e}$, and the estimated values are used as initial models in the inversion.

Figure 5(a) plots the curves of P- and S-wave velocities and density provided by the well log; in Figure 5(b) we plot the computed results of porosity ϕ, clay volume $V_{\rm clay}$ and stress-sensitive parameter $P_{\rm e}$; and the estimated results of bulk moduli of dry rock and fluid ($K_{\rm dry}$ and $K_{\rm f}$) and shear modulus μ are shown in Figure 5(c).

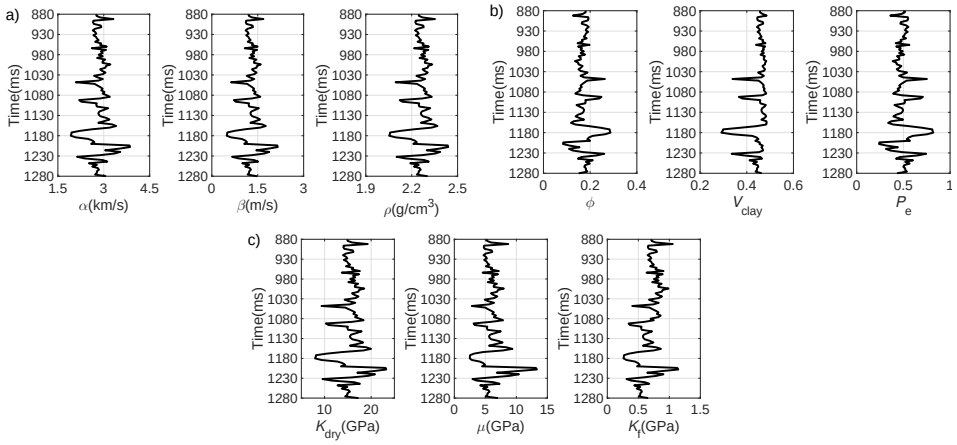

FIG. 5. Constructed well log model. (a) Curves of P- and S-wave velocities and density provided by well log data; (b) Computed results of porosity, clay volume and stress-sensitive parameter; and (c) Calculated results of effective bulk moduli of dry rock and fluid, and shear modulus.

Using a 20 Hz Ricker wavelet, we generate synthetic seismic data employing Zoeppritz equation and the derived reflection coefficient (equation 13) respectively. Figure 6 plots comparison between the generated results. We observe that the synthetic data generated using the derived reflection coefficient match the data obtained using Zoeppritz equation

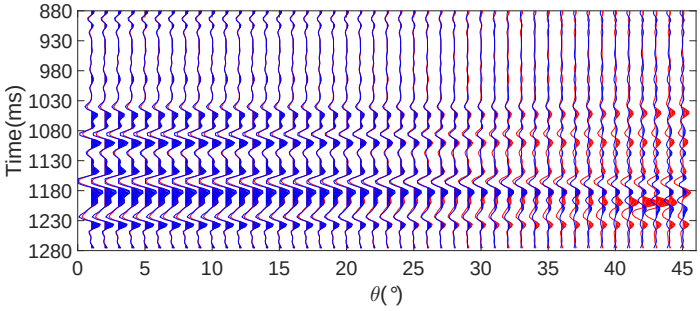

FIG. 6. Comparison between synthetic seismic data generated using Zoeppritz equation (red) and those generated using the derived reflection coefficient (blue).

closely in the case of the maximum incidence angle being around 30°. Therefore we may apply the derived reflection coefficient and the inversion approach proposed based on the derived reflection coefficient to seismic data whose maximum incidence angle is around 30°.

Synthetic test: verification of stability of the proposed inversion approach

We next utilize noisy synthetic seismic data, which are generated using Zoeppritz equation and added with random noise, to verify the robustness and accuracy of the proposed inversion approach. In Figure 7 we plot profiles of noisy seismic data. Signal-to-noise ratio (SNR) is 2, and the incidence angle range is $1^\circ - 30^\circ$. The input for EI inversion is obtained by stacking the pre-stack seismic data over different ranges of incidence angle (i.e. $1^\circ - 6^\circ$, $7^\circ - 12^\circ$, $13^\circ - 18^\circ$, $19^\circ - 24^\circ$, and $25^\circ - 30^\circ$); therefore the incidence angles used in equation 21 are approximately $\theta_1 = 3^\circ$, $\theta_2 = 9^\circ$, $\theta_3 = 15^\circ$, $\theta_4 = 21^\circ$ and $\theta_5 = 27^\circ$.

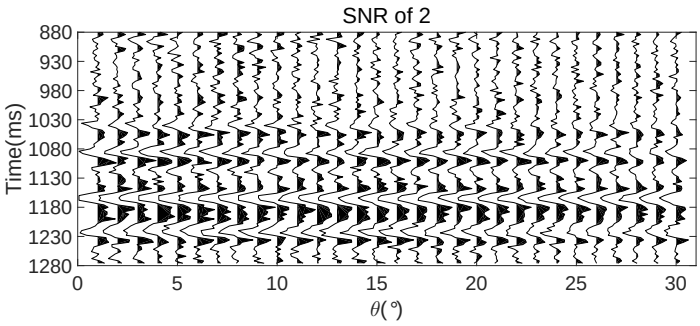

FIG. 7. Profiles of noisy seismic data. The signal-to-noise ratio (SNR) is 2.

We implement the estimation of EI, and plot comparisons between inversion results of EI and values computed using equation 17 in Figure 8. We observe there is a good match between the inversion result and the true value, which indicates the inversion results of EI can be used as a reasonable input in the inversion for unknown parameters.

We apply the proposed inversion approach to the noisy seismic data, and compare inversion results of unknown parameters (K_{dry}, μ, F, K_{f}, and P_{e}) and their corresponding true values (i.e. well log curves plotted in Figure 5), as displayed in Figure 9. Table 1 shows the detailed steps of EI inversion for unknown parameters (i.e. a four-step inversion), in

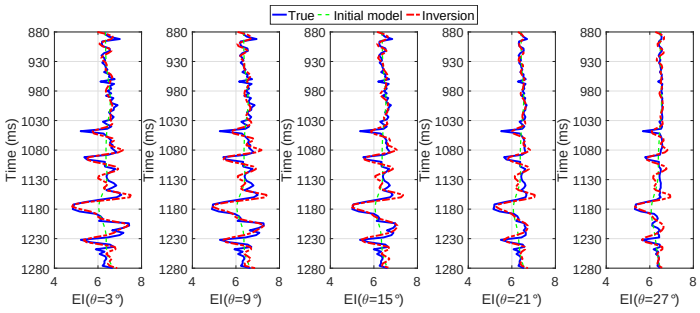

FIG. 8. Comparisons between inversion results and true values of EI.

which we explain how to implement the inversion. From Figure 9 we observe that using the proposed inversion approach can generate inversion results that match true values closely, which may confirm that the proposed approach is stable even in the case of seismic data containing random noise (SNR=2).

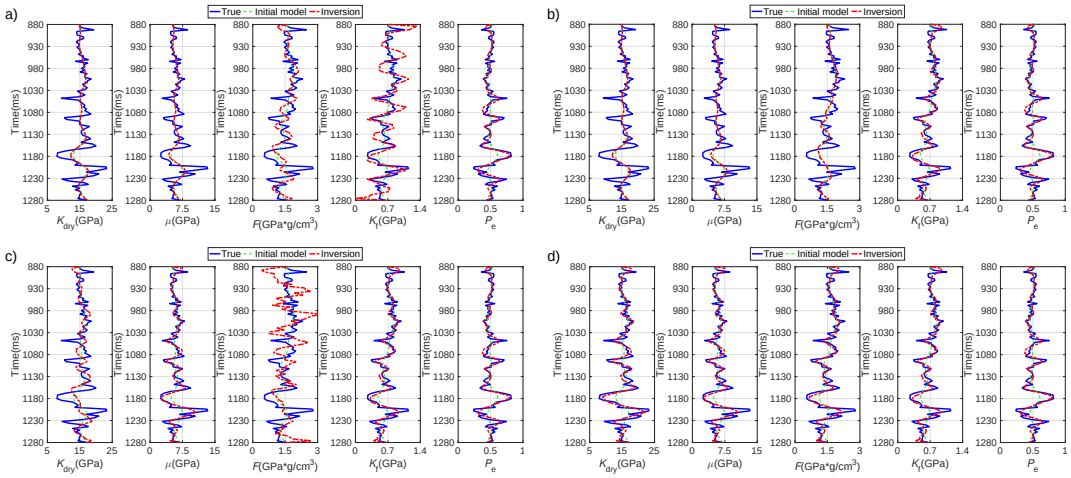

FIG. 9. Comparisons between inversion results and true values. a) Step 1: using $\mathrm{EI}\,(\theta_1)$ to estimate P_e; b) Step 2: using $\mathrm{EI}\,(\theta_2)$ to obtain K_f; c) Step 3: using $\mathrm{EI}\,(\theta_3)$ to estimate μ; d) Step 4: using $\mathrm{EI}\,(\theta_4)$ and $\mathrm{EI}\,(\theta_5)$ to compute K_dry and F.

Table 1. A four-step inversion

Step1	Using $\mathrm{EI}\,(\theta_1)$ to obtain the stress-sensitive parameter P_e;
Step2	Using $\mathrm{EI}\,(\theta_2)$ and the estimated P_e to obtain the fluid bulk modulus K_f;
Step3	Using $\mathrm{EI}\,(\theta_3)$ and the estimated P_e and K_f to obtain the shear modulus μ,
Step4	Using $\mathrm{EI}\,(\theta_4)$ and $\mathrm{EI}\,(\theta_5)$ and the estimated P_e, K_f and μ to obtain the dry rock bulk modulus K_dry and fluid-sensitive parameter F.

Test on a real dataset

Since we have verified the stability of the proposed approach using synthetic data, we proceed to illustrate how to apply the inversion approach to a real data set that is acquired

over a hydrocarbon reservoir to confirm its accuracy and reliability. Figure 10 plots profiles of stacked seismic data ($\theta_1 = 3°$, $\theta_2 = 9°$, $\theta_3 = 15°$, $\theta_4 = 21°$ and $\theta_5 = 27°$), in which P-wave velocity curve is spliced. The arrow in each figure indicates the location of the gas-bearing reservoir. Prior to being used for the inversion, the seismic data have underwent AVO-compliant preprocessing. From Figure 10 we observe that there is a strong reflection around the gas-bearing reservoir.

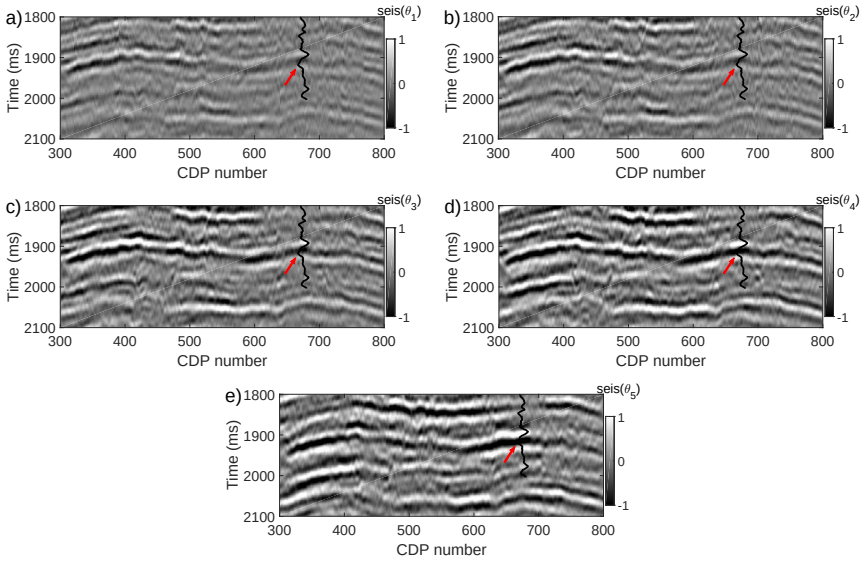

FIG. 10. Profiles of stacked seismic data. The incidence angles are $\theta_1 = 3°$, $\theta_2 = 9°$, $\theta_3 = 15°$, $\theta_4 = 21°$ and $\theta_5 = 27°$. Black curve represents P-wave velocity.

Again using the model-constrained least-square inversion algorithm (Chen et al., 2018), we obtain the inversion results of EI at the corresponding incidence angles, as plotted in Figure 11. We observe that EI exhibits a relatively low value at the location of gas-bearing reservoir.

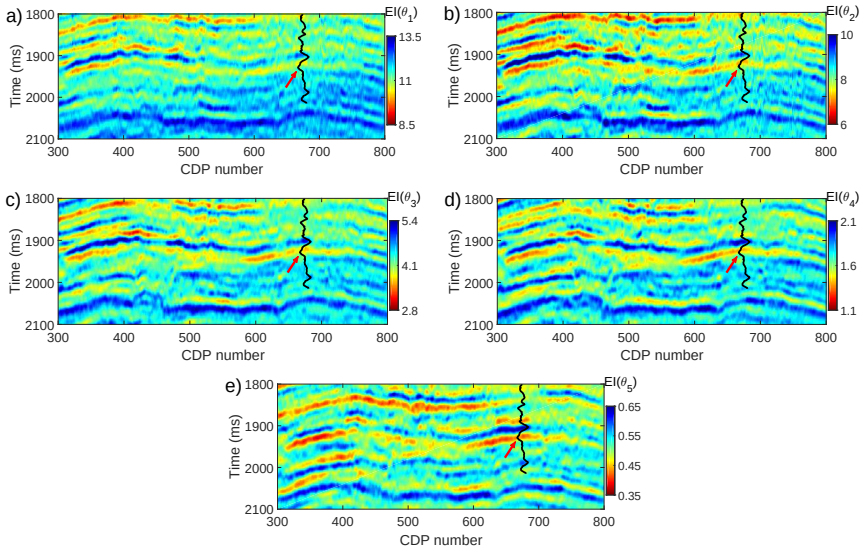

FIG. 11. Inversion results of EI. The incidence angles are $\theta_1 = 3°$, $\theta_2 = 9°$, $\theta_3 = 15°$, $\theta_4 = 21°$ and $\theta_5 = 27°$. Black curve represents P-wave velocity.

With the inversion results of EI in hand, we proceed to the four-step nonlinear inversion for the bulk and shear moduli of dry rock, fluid-sensitive factor and bulk modulus of fluid, and stress-sensitive parameter. For the construction of initial models, a software package is employed to implement a rough estimation of P- and S-wave impedances and density using pre-stack seismic data. Following the procedure presented in the section of well log model construction we also roughly estimate the results of $K_{\rm dry}$, μ, F, $K_{\rm f}$ and $P_{\rm e}$ using results of P- and S-wave velocities and density that are estimated using a commercial software package. The smoothed version of the roughly estimated result is used as the initial model in the nonlinear inversion, as plotted in Figure 12. In Figure 13 we plot the final inversion results of $K_{\rm dry}$, μ, F, $K_{\rm f}$ and $P_{\rm e}$.

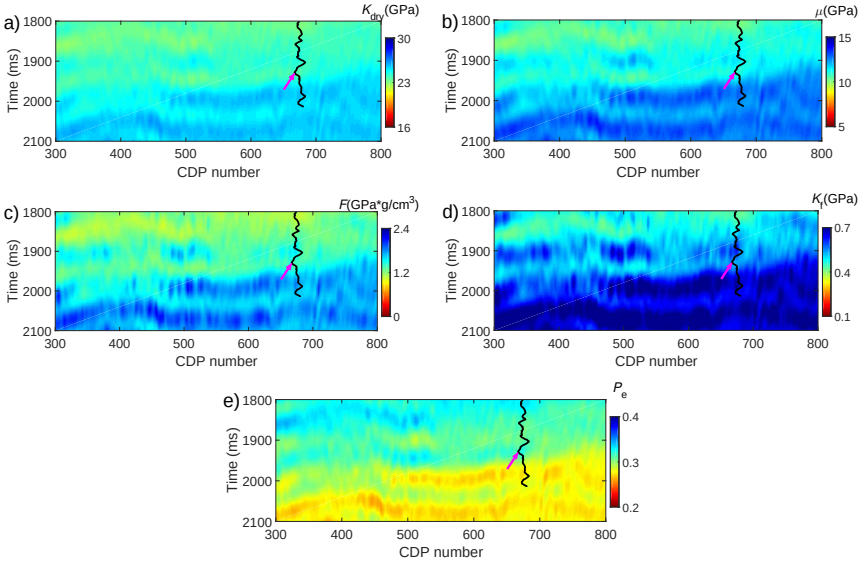

FIG. 12. Initial models of unknown parameters. Black curve represents P-wave velocity.

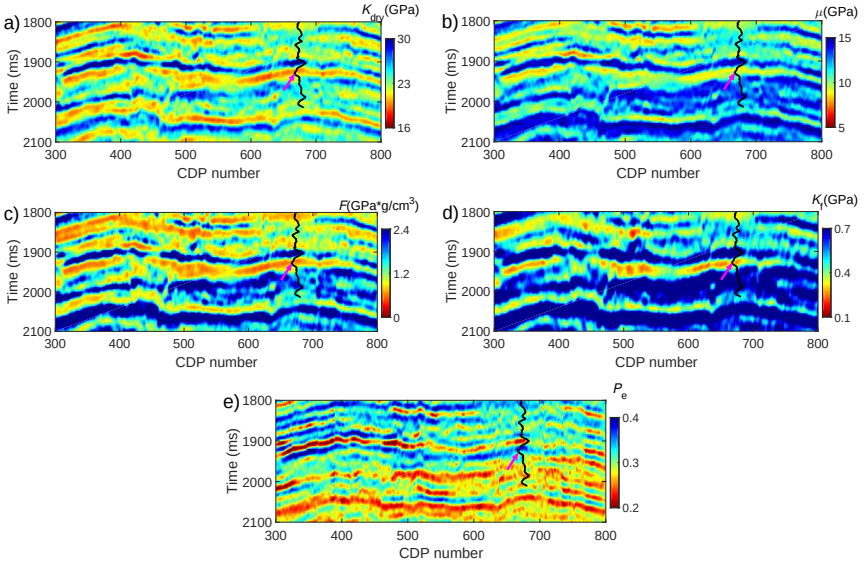

FIG. 13. Inversion results of unknown parameters. Black curve represents P-wave velocity.

We observe that the proposed approach generate inversion results of bulk and shear

moduli of dry rock, fluid factor, bulk modulus of fluid and stress-sensitive parameter, which may match the curve of P-wave velocity well, and we also see that the inversion results of $K_{\rm dry}$, μ, F and $K_{\rm f}$ exhibit relatively low values at the location of the reservoir (as marked by the arrow in each figure) and the estimated stress-sensitive parameter show relatively high values.

DISCUSSIONS

In the present study, there are some conditions and assumptions under which we derive the reflection coefficient and propose the approach of seismic inversion for stress-sensitive parameter. We first obtain an approximation of the Gassmann (1951) fluid substitution equation, and in the approximate equation we introduce a stress-sensitive parameter to replace the porosity term, in which the critical porosity (CP) model is employed to relate the bulk modulus of dry rock to the porosity term. The critical porosity used in the generation of synthetic seismic data and the inversion of real data is approximately 0.35, which is chosen by comparing results computed using the CP model and those calculated using Krief's equation. The approximate value of critical porosity is applicable in the case of the porosity being less than 0.2. In order to obtain a more accurate result of critical porosity, experimental measurements of rock cores are required.

Utilizing perturbations in stiffness parameters derived using the proposed approximate expression of Gassmann's equation, we obtain the linearized expression of reflection coefficient as a function of stress-sensitive parameter. Comparing the reflection coefficient computed using Zoeppritz equation and that calculated using the linearized expression, we confirm that the proposed reflection coefficient is applicable in the case of the maximum incidence angle of seismic data being less than 30°. It indicates that the inversion approach proposed based on the derived reflection coefficient can be applied to the real data whose maximum incidence angle is around 30°.

After transferring the derived reflection coefficient to the corresponding EI, we propose the nonlinear inversion approach of estimating stress-sensitive parameter using observed seismic data. The nonlinear inversion approach is established on the basic of obtaining the result that make the energy of data residual be smaller. In order to verify the accuracy of the inversion approach, we implement the simultaneous inversion for unknown parameters using synthetic seismic data shown in Figure 7. Figure 14 plots comparisons between true values and inversion results obtained using the simultaneous inversion.

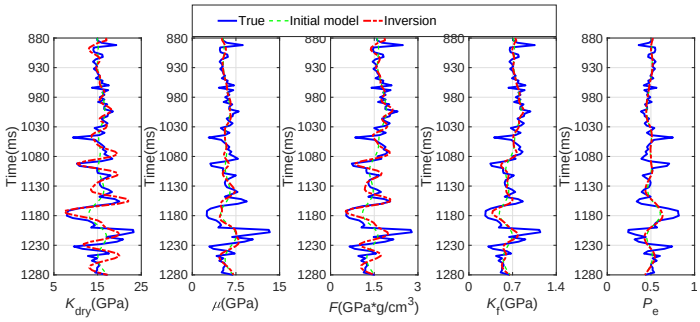

FIG. 14. Comparisons between inversion results and true values of EI.

Comparing the results shown in Figure 9(d) and the results plotted in Figure 14, we observe that the simultaneous inversion may only obtain acceptable results of $K_{\rm dry}$ and F; however, the accuracy of the inversion for other unknown parameters(μ, $K_{\rm f}$ and $P_{\rm e}$) should be improved.

CONCLUSIONS

We first obtain simplification and approximation of fluid substitution equation, in which we introduce a stress-sensitive parameter based on the critical porosity model. From the variation of the stress-sensitive parameter with water saturation and porosity, we conclude that the stress-sensitive parameter exhibits relatively high values in gas-bearing porous reservoirs. Relating stiffness parameters to the stress-sensitive parameters, we express perturbations in stiffness parameters across an interface separating two layers. Using the perturbations, we derive a linearized reflection coefficient in terms of reflectivities of dry rock bulk modulus, shear modulus, fluid-sensitive factor, fluid bulk modulus and stress-sensitive parameter, and we also transfer the derived reflection coefficient to elastic impedance (EI). Comparing results computed using the derived reflection coefficient and Zoeppritz equation, we confirm that the derived reflection is applicable in the case of the maximum incidence angle being around 30°. Based on the expression of EI, we establish a four-step nonlinear inversion approach to estimate dry rock elastic properties, fluid factor, and stress-sensitive parameter.

The stability of the nonlinear inversion is verified using noisy synthetic seismic data generated using Zoeppritz equation. We stress that the datasets stacked over different ranges of incidence angle are employed to estimate results of EI using a least-squares inversion algorithm, and the estimated results of EI preserve as the input in the nonlinear inversion for dry rock elastic properties, fluid factor, and stress-sensitive parameter. Comparing results estimated using the proposed approach and those obtained using the simultaneous inversion, we confirm that the accuracy of the nonlinear inversion for the unknown parameters is relatively higher than that of the simultaneous inversion. Applying the proposed inversion approach to real data that have undergone careful amplitude processing, we conclude the approach appears to provide results that can guide rock-physics interpretation, specifically fluid identification and stress prediction.

ACKNOWLEDGMENTS

The industrial sponsors of the Consortium for Research in Elastic Wave Exploration Seismology (CREWES) are thanked for their support. We gratefully acknowledge additional support from Natural Science and Engineering Research Council of Canada through the grant no. CRDPJ 461179-13. This research was undertaken thanks in part to funding from the Canada First Research Excellence Fund, and the Mitacs Accelerate grant *Responsible Development of Unconventional Hydrocarbon Reserves*. The SINOPEC Key Lab of Multi-Component Seismic Technology is thanked for providing the processed real data. Hampson-Russell software was used for wavelet extraction and implementing the estimation of P- and S-wave velocities and density.

APPENDIX A. EXPRESSIONS OF FRACTURE WEAKNESSES

Following Shaw and Sen (2006), we express ξ_{ij} parameters as

$$\begin{aligned}
&\xi_{11} = \frac{\sin^4\theta\cos^4\phi}{\alpha^2}, \xi_{12} = \frac{\sin^4\theta\sin^2\phi\cos^2\phi}{\alpha^2}, \xi_{13} = \frac{\sin^2\theta\cos^2\theta\cos^2\phi}{\alpha^2}, \xi_{21} = \xi_{12},\\
&\xi_{22} = \frac{\sin^4\theta\sin^4\phi}{\alpha^2}, \xi_{23} = \frac{\sin^2\theta\cos^2\theta\sin^2\phi}{\alpha^2}, \xi_{31} = \xi_{13}, \xi_{32} = \xi_{23}, \xi_{33} = \frac{\cos^4\theta}{\alpha^2},\\
&\xi_{44} = \frac{-4\sin^2\theta\cos^2\theta\sin^2\phi}{\alpha^2}, \xi_{55} = \frac{-4\sin^2\theta\cos^2\theta\cos^2\phi}{\alpha^2}, \xi_{66} = \frac{4\sin^4\theta\sin^2\phi\cos^2\phi}{\alpha^2},
\end{aligned} \tag{A.1}$$

where ($\alpha = \sqrt{\frac{K_{\rm sat}+4/3\mu}{\rho}}$ and $\beta = \sqrt{\frac{\mu}{\rho}}$). Combining equations 9-12 and A.1, we obtain

$$\begin{aligned}
R_{\rm PP} &= \frac{1}{4\rho\cos^2\theta}\left(\Delta\rho\cos 2\theta + \frac{\rho\Delta C_{33}}{K_{\rm sat}+4/3\mu} - \frac{8\rho\sin^2\theta\cos^2\theta\Delta C_{55}}{K_{\rm sat}+4/3\mu}\right)\\
&= \frac{\Delta\rho\cos 2\theta}{4\rho\cos^2\theta} + \frac{1}{4\cos^2\theta}\left(\begin{array}{l}\frac{\Delta K_{\rm dry}}{K_{\rm dry}}\frac{K_{\rm dry}}{K_{\rm sat}+4/3\mu}\\ +\frac{K_{\rm f}}{K_{\rm sat}+4/3\mu}\frac{\Delta K_{\rm f}}{K_{\rm f}}\frac{P_{\rm e}}{\phi_{\rm c}}\\ +\frac{P_{\rm e}}{K_{\rm sat}+4/3\mu}\frac{K_{\rm f}}{\phi_{\rm c}}\frac{\Delta P_{\rm e}}{P_{\rm e}}\end{array}\right) - 2\gamma_{\rm sat}\sin^2\theta\frac{\Delta\mu}{\mu}\\
&= \frac{\Delta\rho\cos 2\theta}{4\rho\cos^2\theta} + \frac{1}{4\cos^2\theta}\left(\frac{\gamma_{\rm sat}}{\gamma_{\rm dry}} - \frac{4}{3}\gamma_{\rm sat}\right)\frac{\Delta K_{\rm dry}}{K_{\rm dry}} + \frac{1}{4\cos^2\theta}\left(1 - \frac{\gamma_{\rm sat}}{\gamma_{\rm dry}}\right)\frac{\Delta K_{\rm f}}{K_{\rm f}}\\
&\quad + \frac{1}{4\cos^2\theta}\left(1 - \frac{\gamma_{\rm sat}}{\gamma_{\rm dry}}\right)\frac{\Delta P_{\rm e}}{P_{\rm e}} - 2\gamma_{\rm sat}\sin^2\theta\frac{\Delta\mu}{\mu}\\
&= \frac{1}{4\cos^2\theta}\left(\frac{\gamma_{\rm sat}}{\gamma_{\rm dry}} - \frac{4}{3}\gamma_{\rm sat}\right)\frac{\Delta K_{\rm dry}}{K_{\rm dry}} - 2\gamma_{\rm sat}\sin^2\theta\frac{\Delta\mu}{\mu} + \frac{\cos 2\theta}{4\cos^2\theta}\frac{\Delta F}{F}\\
&\quad + \left[\frac{1}{2}\tan^2\theta - \frac{1}{4\cos^2\theta}\left(\frac{\gamma_{\rm sat}}{\gamma_{\rm dry}}\right)\right]\frac{\Delta K_{\rm f}}{K_{\rm f}} + \frac{1}{4\cos^2\theta}\left(1 - \frac{\gamma_{\rm sat}}{\gamma_{\rm dry}}\right)\frac{\Delta P_{\rm e}}{P_{\rm e}},
\end{aligned} \tag{A.2}$$

where F is a fluid-sensitive factor, $F = \rho K_{\rm f}$, $\gamma_{\rm sat} = \mu/\left(K_{\rm sat}+4/3\mu\right)$, and $\gamma_{\rm dry} = \mu/\left(K_{\rm dry}+4/3\mu\right)$, respectively.

REFERENCES

Athy, L. F., 1930, Density, porosity, and compaction of sedimentary rocks: AAPG Bulletin, **14**, No. 1, 1–24.

Blangy, J.-P., 1992, Integrated seismic lithology interpretation: the petrophysical basis: Ph.D. thesis, Stanford University.

Castagna, J. P., Batzle, M. L., and Eastwood, R. L., 1985, Relationships between compressional-wave and shear-wave velocities in clastic silicate rocks: Geophysics, **50**, No. 4, 571–581.

Chen, H., Innanen, K. A., and Chen, T., 2018, Estimating p-and s-wave inverse quality factors from observed seismic data using an attenuative elastic impedance: Geophysics, **83**, No. 2, R173–R187.

Connolly, P., 1999, Elastic impedance: The leading edge, **18**, No. 4, 438–452.

Gassmann, F., 1951, Über die elastizität poröser medien: Vier. der Natur. Gesellschaft Zürich, **96**, 1–23.

Hantschel, T., and Kauerauf, A. I., 2009, Fundamentals of basin and petroleum systems modeling: Springer Science & Business Media.

Innanen, K. A., 2014, Seismic avo and the inverse hessian in precritical reflection full waveform inversion: Geophysical Journal International, **199**, No. 2, 717–734.

Köhn, D., 2011, Time domain 2d elastic full waveform tomography: Ph.D. thesis, University of Kiel.

Krief, M., Garat, J., Stellingwerf, J., and Ventre, J., 1990, A petrophysical interpretation using the velocities of p and s waves (full-waveform sonic): The Log Analyst, **31**, No. 06.

Mavko, G., Mukerji, T., and Dvorkin, J., 2009, The rock physics handbook: Tools for seismic analysis of porous media: Cambridge university press.

Nur, A., Mavko, G., Dvorkin, J., and Galmudi, D., 1998, Critical porosity: A key to relating physical properties to porosity in rocks: The Leading Edge, **17**, No. 3, 357–362.

Pan, W., Geng, Y., and Innanen, K. A., 2018, Interparameter trade-off quantification and reduction in isotropic-elastic full-waveform inversion: synthetic experiments and hussar land data set application: Geophysical Journal International, **213**, No. 2, 1305–1333.

Pan, W., Innanen, K. A., and Liao, W., 2017, Accelerating hessian-free gauss-newton full-waveform inversion via l-bfgs preconditioned conjugate-gradient algorithm: Geophysics, **82**, No. 2, R49–R64.

Shaw, R. K., and Sen, M. K., 2006, Use of avoa data to estimate fluid indicator in a vertically fractured medium: Geophysics, **71**, No. 3, C15–C24.

Smith, J., 1971, The dynamics of shale compaction and evolution of pore-fluid pressures: Journal of the International Association for Mathematical Geology, **3**, No. 3, 239–263.

Whitcombe, D. N., 2002, Elastic impedance normalization: Geophysics, **67**, No. 1, 60–62.

Zoback, M. D., 2010, Reservoir geomechanics: Cambridge University Press.